Solid State Sciences 13 (2011) 2030–2036

Contents lists available at SciVerse ScienceDirect

Solid State Sciences

journal homepage: www.elsevier.com/locate/ssscie

Structural, microstructural and Mössbauer study of $BiFeO_3$ synthesized at low temperature by a microwave-hydrothermal method

J. Prado-Gonjal[a], D. Ávila[a], M.E. Villafuerte-Castrejón[b], F. González-García[c], L. Fuentes[d], R.W. Gómez[e], J.L. Pérez-Mazariego[e], V. Marquina[e], E. Morán[a,*]

[a] Departamento de Química Inorgánica, Facultad de Ciencias Químicas, UCM, 28040 Madrid, Spain
[b] Instituto de Investigaciones en Materiales, Universidad Nacional Autónoma de México, AP 70360, México DF 4510, Mexico
[c] Departamento de Ingeniería de Procesos e Hidráulica, Universidad Autónoma Metropolitana-Iztapalapa, A. Postal 55-534, México DF 09340, Mexico
[d] Centro de Investigación en Materiales Avanzados CIMAV, Miguel de Cervantes 120, Chihuahua 31109, Mexico
[e] Facultad de Ciencias, Universidad Nacional Autónoma de México, México DF 04510, Mexico

ARTICLE INFO

Article history:
Received 5 August 2011
Received in revised form
13 September 2011
Accepted 15 September 2011
Available online 22 September 2011

Keywords:
BiFeO3
Microwave processing
Electron microscopy
X-ray methods
Mössbauer spectroscopy

ABSTRACT

Multiferroic $BiFeO_3$ has been rapidly synthesized by a microwave – hydrothermal method using nitrates as the metallic source. Structural characterization was performed by thermal analysis, X-ray diffraction and transmission electron microscopy. Generally accepted trigonal space group R3c, as well as recently suggested monoclinic symmetries, were assayed in the search for the best fit. Due to the ambiguity of the Rietveld refinement to distinguish between crystal systems, a micro-diffraction and HRTEM study has been performed. The best solution was obtained with the trigonal model. The room-temperature Mössbauer spectra reveal the presence of a small fraction (2%) of iron in low spin configuration.

1. Introduction

Multiferroics are materials in which two or three ferroic orders (ferroelectric, ferromagnetic and/or ferroelastic) occur in the same phase. This class of materials is worth being investigated on account of its potential applications in spintronics, memory devices and magnetoelectric systems. $BiFeO_3$ (BFO) is an interesting magnetoelectric multiferroic because its ferroelectric and antiferromagnetic ordered conditions take place concurrently at room temperature [1]. It is described as a rhombohedrally distorted ferroelectric perovskite (Tc ≈ 1100 K) with G-type canted antiferromagnetism up to 643 K (T_N), in which all neighboring magnetic spins are oriented antiparallel to each other. The Fe^{3+} ions in $BiFeO_3$ have d^5 electron configuration, so ferroelectricity is almost certainly driven by the Bi^{3+} lone pairs [2,3].

In spite of the plethora of work accumulated on $BiFeO_3$ there are a few problems not yet solved. A main one concerns its synthesis, which is currently done by the high temperature ceramic method but presenting many drawbacks. For example, for synthesizing $BiFeO_3$, the kinetics of phase formation in the Bi_2O_3–Fe_2O_3 system can easily lead to the appearance of secondary phases such as Bi_2O_3, mullite-type $Bi_2Fe_4O_9$, and sillenite-type $Bi_{25}FeO_{39}$ [4]. Besides the solid state route, several techniques have been used to prepare this material: anodized alumina templates, wet chemical routes, rapid sintering process, hydrothermal methods, etc. [5–11]. In order to obtain a pure phase, the temperature and time of the heat treatment are critical. For instance, more than 1 h treatment at 600 °C induces decomposition of the compound. $BiFeO_3$ is a metastable phase at this temperature and decomposes according to the reaction

$$49\ BiFeO_3 \rightarrow 12\ Bi_2Fe_4O_9 + Bi_{25}FeO_{39},$$

so one must take care to avoid long heat treatments [12]. According to all versions of published binary phase diagrams [13,14], these phases are not thermodynamically compatible. Moreover, at higher temperatures phase transitions take place: a transition to a $GdFeO_3$-type orthorhombic phase (the β-polymorph) has been reported to occur at 825 °C (close to, or associated to the para-ferroelectric transition) and a third cubic polymorph (the elusive

* Corresponding author. Tel.: +34 913944234; fax: +34 913944352.
E-mail address: emoran@quim.ucm.es (E. Morán).

1293-2558/$ – see front matter © 2011 Elsevier Masson SAS. All rights reserved.
doi:10.1016/j.solidstatesciences.2011.09.006

"γ-phase") has been claimed [15]. Taking all of this into account it is clear that a low temperature synthesis method for $BiFeO_3$, as the one reported by our group using microwave-hydrothermal synthesis (200 °C) is very convenient [16]. Moreover, with this technique it was demonstrated that the successful synthesis of single phase powder $BiFeO_3$ by microwave-hydrothermal method is not dependent on the purity of the starting reactants [17].

Another kind of problems in $BiFeO_3$ are related to cationic valences and oxygen stoichiometry because Fe^{2+} can be easily formed if accompanied by oxygen vacancies to keep the charge balance, with a concomitant degradation of the magnetic and electric properties.

Concerning crystallographic features, for $BiFeO_3$, although the generally accepted structure is trigonal, with space group # 161 (R3c) [18], a distorted tetragonal phase (P4mm) has been identified in thin films under strain [19]. Besides, the chemical doping can also stabilize new phases of the same material. For example, it has been recently reported that the solid solution $0.8BiFeO_3$–$0.2BaTiO_3$ processed by high energy ball milling yields a monoclinic phase (S G #8 cm) [20].

Thus, the aim of this work, taking into account the fact that low temperature synthetic methods could stabilize different polymorphs, is to ascertain the space group and to deep into the microstructural study of a $BiFeO_3$ prepared as a single phase by a new, low temperature, "fast chemistry" and fully reproducible method: the microwave-hydrothermal synthesis. Last but not least, Mössbauer spectroscopy has been performed, both in the as-prepared and oxidized materials, in order to deep in the oxidation states and spin configurations of iron.

2. Experimental

Synthesis was performed by the microwave-hydrothermal method recently reported by Prado-Gonjal et al. [16]: a fully automated commercial Milestone ETHOS 1 apparatus, operating at 2450 MHz, with programmed pressure, power–temperature and time, equipped with a stirrer motor and a twist board, was used. Initial reactants were $Bi(NO_3)_3 \cdot 5H_2O$ (Merck, 98%) and $Fe(NO_3)_3 \cdot 9H_2O$ (Merck, 98%) in 20 ml KOH 4M. The reactions were carried out in double-walled vessels consisting of an inner Teflon container (100 ml) and an outer shell of high strength polymer. The heating program used was as follows: heating up to 200 °C for 15 min, a 30 min dwell at this temperature and switching off the power to cool down at room temperature. The pressure limit was set at 15 bars – close to the autogenous vapor pressure – and the power limited to 500 W, keeping the system under vigorous agitation. Finally, the products were decanted and leached with HNO_3 2 M, water rinsed to eliminate remaining impurities, and dried at 100 °C in a conventional oven. To oxidize the iron atoms from Fe^{2+} to Fe^{3+}, the sample was heat treated at 300 °C during 3 h in flowing oxygen.

Room temperature X-ray diffraction was performed on an X'Pert MPD Philips Instrument diffractometer, working at 45 kV and 40 mA. Cu Kα1 radiation was obtained by means of a Cu curved monochromator. Measurement interval was $5\ ^\circ < 2\theta < 120\ ^\circ$ with step size $\Delta(2\theta) = 0.017^\circ$. Intense reflections in the diffraction pattern showed maxima with intensities of the order of 10^4 counts, corresponding to random errors ~1%. Rietveld analysis of experimental data was performed using the FullProf software [21,22]. Zero shift, lattice parameters, background, peak width, shape and asymmetry, atomic positions and isotropic temperature factors were refined. Symmetry group-subgroup transformations were analyzed via software Powder Cell [23]. Thermal analysis (DTA) was performed in TA Instruments apparatus (SDT Q600 model). Samples for Transmission Electron Microscopy (TEM) were prepared by ultrasonic dispersion of the powder in n-butanol. Drops of this dispersion were deposited on a carbon-coated copper grid. A JEOL 2000FX equipped with a LINK ISIS 300 analyzer has been used for selected area electron diffraction (SAED) and micro-diffraction. HRTEM was performed using a JEOL 3000F TEM yielding an information limit of 1.1 Å. The exit wave has been reconstructed from the focal series

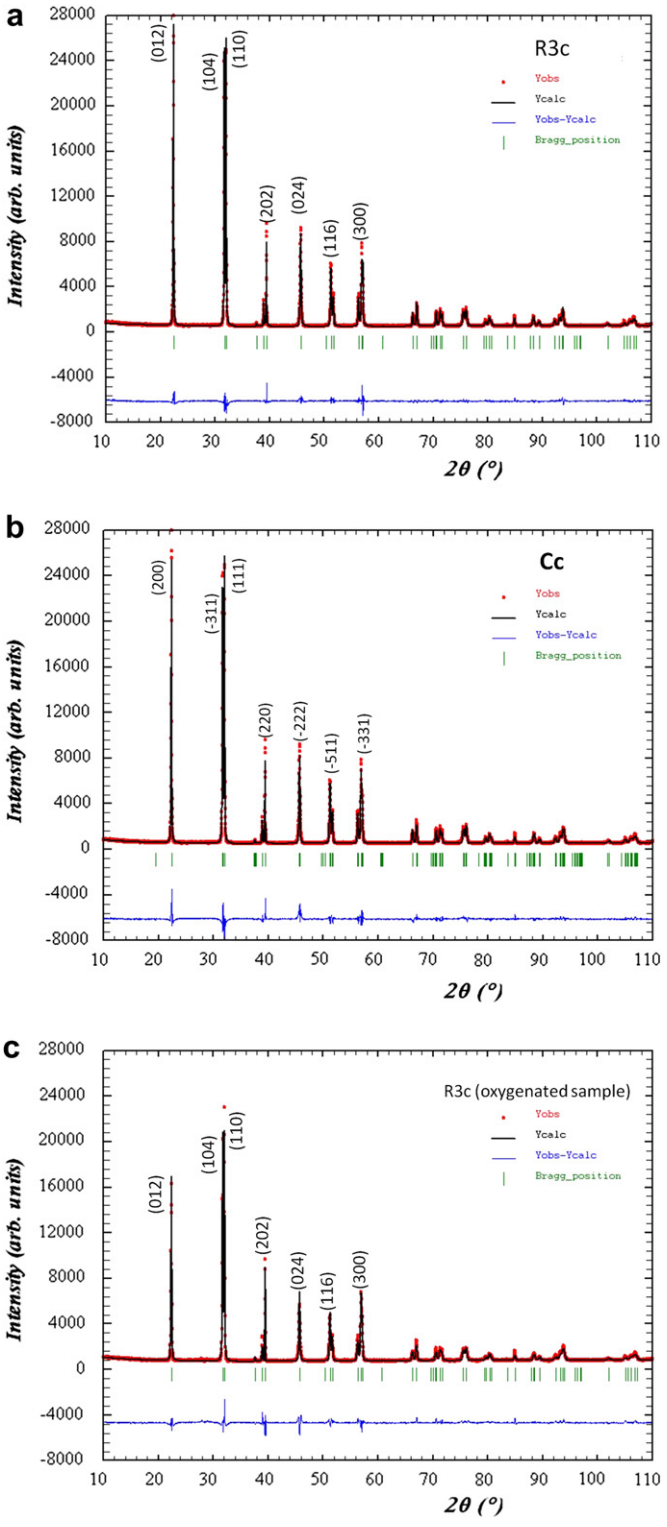

Fig. 1. Rietveld refinement: Observed and calculated diffraction patterns of $BiFeO_3$ a) R3c space group b) Cc space group c) R3c space group of the oxygenated sample.

Table 1
Cell and atomic parameters of $BiFeO_3$ obtained from Rietveld refinement.

Cell parameters: space group R3c (hexagonal system description)					
a = b = 5.58067(5) Å c = 13.8724(1) Å			α = β = 90 ° γ = 120 °		
Atomic parameters					
Name	x	y	z	B	SOF
Bi	0.0000	0.0000	0.0000	0.48(2)	1.00
Fe	0.0000	0.0000	0.7210 (2)	0.77(7)	1.00
O	0.909 (1)	0.203 (1)	0.6205 (5)	0.2	1.00

using the IWFR software [24]. HRTEM images simulations were performed with the MacTempas software [25]. Transmission room temperature Mössbauer spectra of thin powdered absorbers of the samples were recorded with a constant acceleration spectrometer using a ^{57}Co source (1679 MBq) in rhodium matrix. The spectra were fitted with the Recoil 1.05 program [26]. Magnetic susceptibility measurements were performed in a Quantum Design XL-SQUID magnetometer in the temperature range of 2–300 K at 1000 Oe magnetic field. The temperature dependence of the magnetization has been measured following Zero Field Cooled and Field Cooled (ZFC–FC) procedures. The magnetic hysteresis cycles have been recorded at 5 K from magnetization vs applied field measurements.

3. Results and discussion

3.1. Rietveld analysis

Generally accepted [18] trigonal space group # 161 (R3c), as well as recently suggested [19] monoclinic symmetries [# 8 (Cm) and #9 (Cc)], were assayed in the search for the best fit.

The best observed-calculated fitting, shown in Fig. 1a, was obtained with the trigonal R3c model. The number of refined parameters (structural and instrumental) was 26 and Table 1 shows the results of the performed structural analysis. Numbers in parentheses represent standard deviations. The absence of parentheses means that the considered quantity remained fixed during the refinement. The coordinates of bismuth atoms, which are located at high-symmetry sites, were taken as reference. The oxygen temperature factor did not show stability and it was fixed during the refinement. Final reliability factors were: $R_{wp} = 6.23$; $\chi^2 = 3.16$. Refinement results using monoclinic Cm and Cc models lead to worse reliability factors, specifically $R_{wp} \approx 6.6$; $\chi^2 \approx 4.5$, but the difference is not large enough to fully discriminate the monoclinic symmetry (Fig. 1b). Correction of intensities to counterbalance the influence of preferred orientation is necessary. Preferred orientation can be easily recognized on powder diffraction in (012) reflexion for R3c or (200) for Cc (Fig. 1a and b). Hence, electron microscopy has been used, as described in what follows, as a powerful and complementary structural tool to unambiguously find the true symmetry. Taking all this into account, Rietveld refinement for the sample after heating in oxygen atmosphere, was performed using the R3c space group. There is no evidence of texture in the oxygenated sample (Fig. 1c).

3.2. Electron microscopy characterization

Due to the ambiguity of the X-ray to distinguish between both crystal systems, a transmission electron microscopy study has been performed. The SAED (Selected Area Electron Diffraction) study of the reciprocal space (Fig. 2) shows that the reflection conditions are consistent either with trigonal space group R3c (hexagonal unit cell $a_o = b_o = 5.58$ Å and $c_o = 13.87$ Å) or with monoclinic Cc ($a = 9.80$ Å b = 5.57 Å, $c = 5.62$ Å and $\beta = 125$ °). The semi-quantitative XEDS (X-ray energy dispersive spectroscopy) analysis of the composition over 10 crystals yields an average composition of $Bi_{0.98(4)}Fe_{0.99(3)}$, very close to the nominal one.

Choosing between a trigonal cell and a monoclinic one is actually just a convention, because both cells are equivalent. R3c is a minimal non isomorphic supergroup of index 3 of the Cc space group [27] and SAED would never distinguish between both cases, because the same reflections would be present, with the same spacing, changing only the nomenclature of the *hkl* indices, e.g., the 001 monoclinic cell reflection would be equivalent to the −1102 trigonal cell reflection (see Fig. 2).

In order to distinguish them a micro-diffraction analysis is required. Micro-diffraction patterns allow one to obtain the crystal system by employing the "net" symmetry, which is that of a lattice created from the reflections in the pattern. Since the "net" symmetry of the reciprocal lattice depends on the crystal system, the "net" symmetries of the micro-diffraction patterns are directly connected with the crystal system [28].

In Fig. 3, the micro-diffraction pattern from the $[0001]_R$ or $[-101]_m$ is displayed. The zero order Laue zone (ZOLZ) net symmetry for a trigonal system along [0001] is (6mm) whereas it must be (2mm) along [u0w] in the monoclinic case (see Table of Fig. 3). The ZOLZ symmetry observed in the experimental pattern is (6mm) indicating that the true crystal symmetry is trigonal.

The absence of extra reflections or streaking in SAED patterns indicates a well-ordered structure. In order to confirm the degree of ordering of this material, an HREM study was carried out.

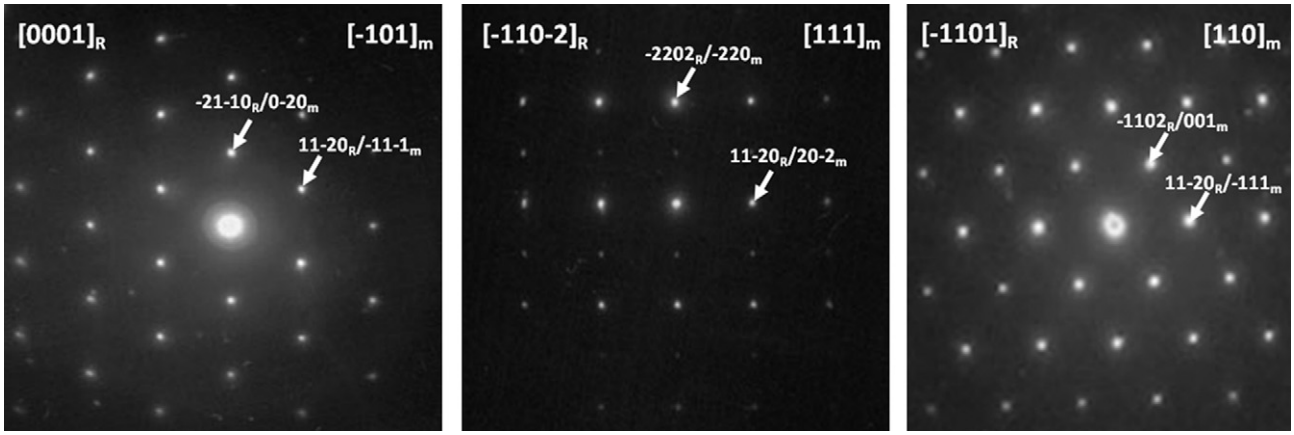

Fig. 2. SAED patterns along the zone axes $[0001]_R/[-101]_m$, $[-110-2]_R/[111]_m$, $[-1101]_R/[110]_m$ of $BiFeO_3$. The subscripts R and m define trigonal and monoclinic symmetry respectively.

Space Group	Net Symmetry in ZOLZ	
	[0001]	[-101]
R3c	(6mm)	
Cc		(2mm)

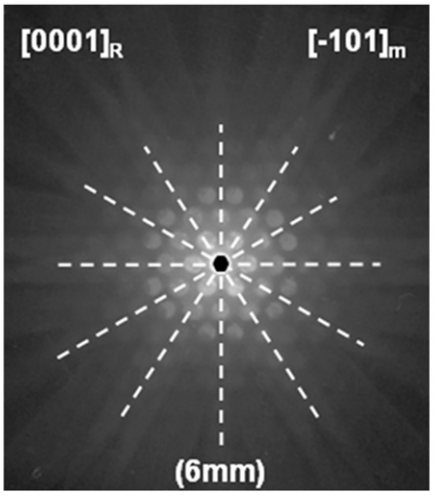

Fig. 3. Microdiffraction pattern along $[0001]_R/[-101]_m$ zone axis showing net symmetry (6mm) in the ZOLZ. The table has been created using the relationships of Table 2 in Ref. [28] (Morniroli, Steeds).

A conventional HRTEM image was recorded along the [−220−1] zone axis (Fig. 4a). In that HREM image, taken near the Scherzer defocus, only the heavy Bi and Fe atoms are visible as dark blobs, in addition we observe a good matching of the calculated image using the structural model refined by X-ray data, squared in yellow, for a defocus value $\Delta f = -400$ Å and a thickness $t = 30$ Å. The main disadvantage of conventional HRTEM is that the resolution is limited by the Scherzer point-resolution, but for a coherent electron source (field emission gun) the information limit of the microscope reaches beyond this point-resolution. In this sense the Exit Wave Reconstruction using a set of images taken at different defocus values allows to reach not only the resolution limit of the microscope but also to image light elements, such as oxygen, in presence of heavy cations on the phase image of the restored exit wave (i.e., the electron wave leaving the specimen). In Fig. 4b the phase image of the restored wave-function from the same area imaged in Fig. 4a shows the improvements in resolution details previously described. The enlargement (Fig. 4c) of the area squared in Fig. 4b, clearly reveals the light oxygen columns (grey blobs) together with those corresponding to the heavy Bi and Fe cations (white dots). Notice that the arrangement of the dots reproduces very well the atomic positions of the different atomic columns (Bi in yellow, Fe in green and O in orange) in the projected structural model. This structural image allows us to confirm the absence of any distortion yielding the trigonal symmetry as it has been observed in thin films [19].

3.3. DTA analysis

Fig. 5 shows the DTA curve for $BiFeO_3$ in the 500 °C–1000 °C interval, where three endothermic peaks are observed. The first one appears at 821 °C and has been reported as the ferroelectric phase

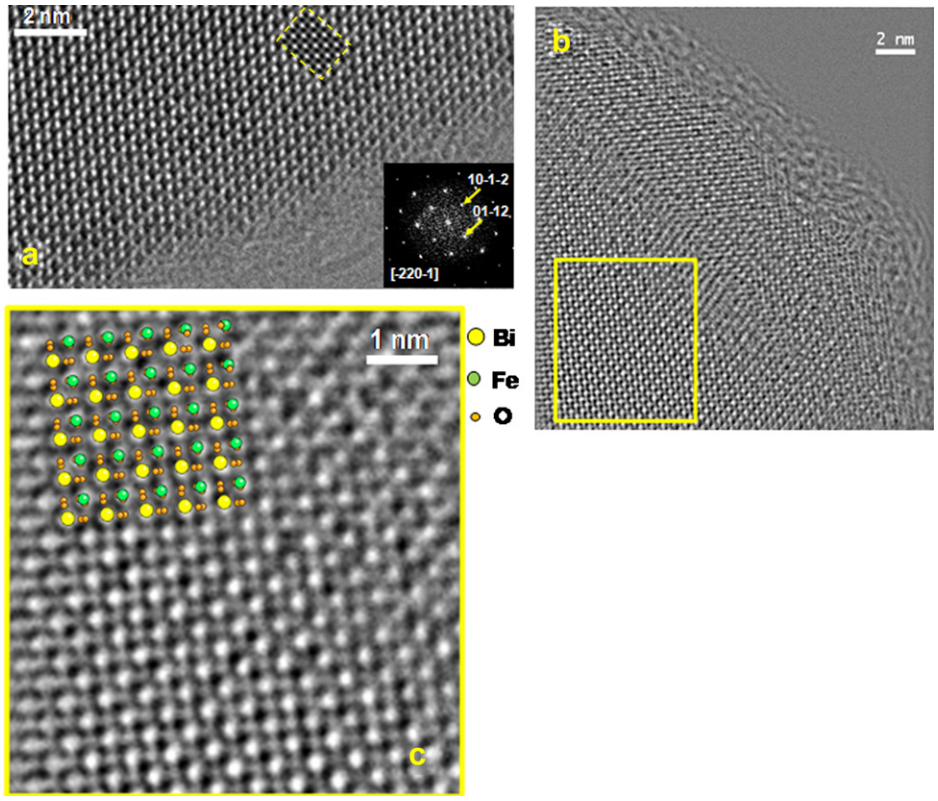

Fig. 4. a) Conventional HRTEM image from a thin crystal of $BiFeO_3$ along [−220−1] showing the cation arrangement, and the good agreement with the calculated one. b) Phase of the reconstructed exit wave function from a focal series of a different area of the same specimen with all the cations and anions resolved. c) Enlargement of the squared yellow area of b) with the projected atomic model overlapped. (For interpretation of the references to colour in this figure legend, the reader is referred to the web version of this article.)

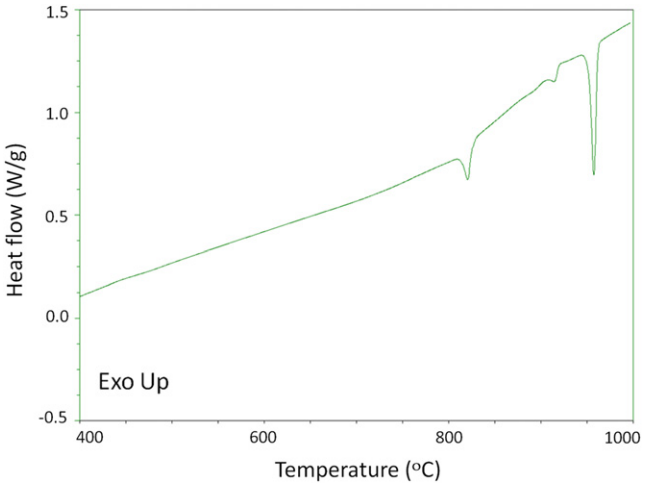

Fig. 5. DTA curve for $BiFeO_3$ measured from 400 to 1000 °C.

transition. The one at 915 °C corresponds to the incongruent melting temperature of $BiFeO_3$, and the endothermic peak at 957 °C correspond to the incongruent melting point of $Bi_2Fe_4O_9$ phase, which is formed at high temperature. Nevertheless, the AFM-paramagnetic transition reported to happen at about 370 °C does not appear in our plot, probably due to the small amount of energy involved. All these features are in good agreement with reported data where the magnetic and electric transitions are, to our knowledge, separately shown [12].

3.4. Mössbauer spectroscopy

The room temperature Mössbauer spectra of the samples appear to be the superposition of a magnetic sextet and a quadrupole doublet. However a closer look to the higher velocity lines reveals asymmetries that suggests more than one sextet in the spectra, so the fittings were made with two close sextets and a quadrupole doublet. The results of the fittings are shown in Fig. 6 and the corresponding Mössbauer parameters are listed in Table 2; the isomer shifts are quoted respect to iron. The joint values of the isomer shift and quadrupole splitting of the two sextets correspond to Fe^{3+}; however, these same parameter values for the doublet do not discriminate between low spin configurations of Fe^{3+} ($S = ½$) or Fe^{2+} ($S = 0$).

Although there is only one site in the (trigonal) crystal structure where the iron atoms reside, a magnetic anisotropy has been observed in the NMR spectrum of this compound by Zalesky et al. [29], probably caused by a spiral magnetic phase of $BiFeO_3$, in which the spin distribution density varies along the propagation of a spin modulated magnetic structure, or by an interaction between different electric field gradients originated by structural distortions, or by both. A. Palewicz et al. [30] confirm the results of Zalesky et al. [29]. The anisotropy parameter value obtained by their measurements of the two average hyperfine magnetic fields H_{max}/H_{min} is 0.91 and 0.90, respectively.

One of our results shows that the magnitude of the quadrupole doublet diminishes when the sample is maintained in flowing oxygen, implying a higher symmetry around the iron atoms. In a fully oxygenated sample, the iron atoms are surrounded by six oxygen atoms in a distorted octahedron, giving rise to a relatively small quadrupole splitting; however, if there is an oxygen deficiency, the structure loses symmetry and the quadrupole splitting must have a higher value, which is the case. This result indicates that the ionic state of the iron atoms responsible for the quadrupole

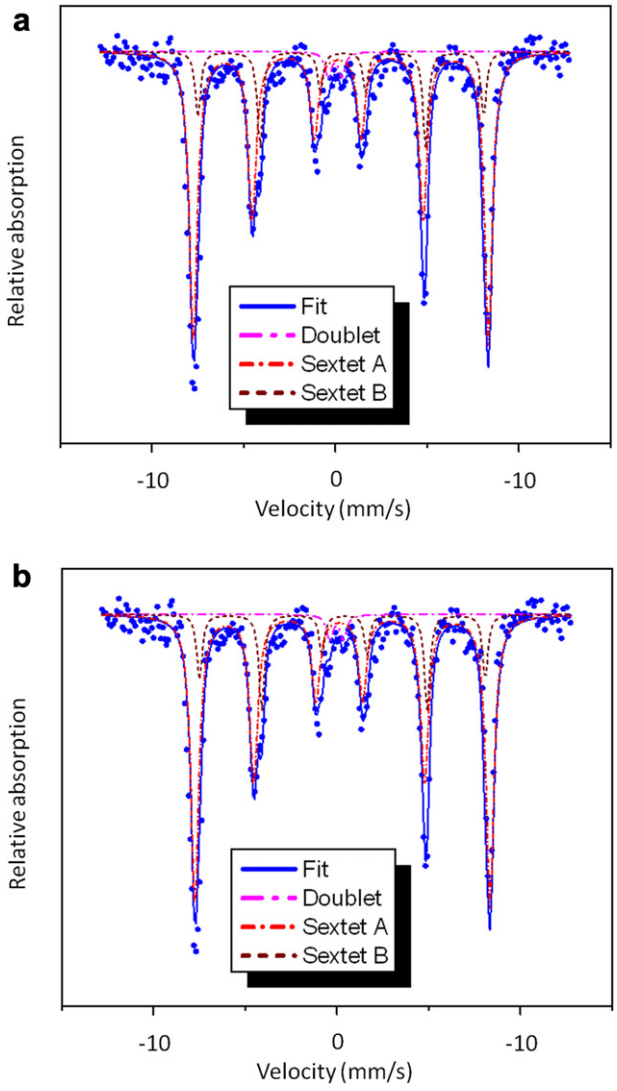

Fig. 6. a)Mössbauer spectrum of the pristine sample. b)Mössbauer spectrum of the oxygenated pristine sample.

doublet in the pristine sample is Fe^{2+} in a low spin configuration. It is likely that, after the heat treatment in flowing oxygen, the oxygen vacancies are occupied changing the ionic state of the iron atoms to Fe^{3+}, maintaining the low spin configuration, and hence giving rise to a smaller quadrupole doublet without changing its relative population.

The other important result is that the relative population between the magnitudes of the magnetic sextets in the pristine sample is 0.24 whereas in the oxygenated sample is 0.97. After the oxygenation one should expect that a modification in the structural distortions affecting the spiral magnetic phase of $BiFeO_3$. When the

Table 2
Mössbauer parameters. Isomer shifts are given respect to metallic iron.

Sample		IS(mm/s)	ΔQ(mm/s)	H (T)	Site (%)
BFO as prepared	Doublet	0.11	0.75	–	2.80
	Sextet A	0.34	0.09	49.85	78.00
	Sextet B	0.48	–0.06	48.28	19.20
BFO after oxidation	Doublet	0.16	0.38	–	2.80
	Sextet A	0.32	0.09	50.50	48.20
	Sextet B	0.46	0.01	49.00	49.00

pristine sample is oxygenated, the corresponding relative intensities becomes close to the value obtained in [29] and [30], indicating that the main cause of the asymmetries is the spiral magnetic phase, in accordance their conclusions.

Another possible origin for the quadrupole doublet could be the presence of a small fraction (~3%) of $BiFeO_3$ nanoparticles small enough so as to become superparamagnetic. Our Mössbauer spectrum is similar to the one obtained by Tae-Jim Park et al. [31] for 51 nm crystals; actually, the Mössbauer parameters that we obtain for the quadrupole doublet are almost exactly equal to the ones they obtain. At present we cannot discriminate between the oxygen deficient surrounding of Fe^{2+} (or Fe^{3+}) in low spin configuration and superparamagnetic $BiFeO_3$ nanoparticles.

3.5. Magnetic properties

The observed magnetic behavior for the as prepared microwave-hydrothermal samples (Fig. 7a) is similar to that reported by S. Basu et al for hydrothermally synthesized samples [32]. The inset shows the temperature dependence of the inverse of susceptibility ($1/\chi$). The $1/\chi$ versus T curve in the paramagnetic state follows the Curie–Weiss law: $\chi = C/(T-\theta)$. A fitting was carried out and it is indicated by a solid line in the inset of Fig. 7a.

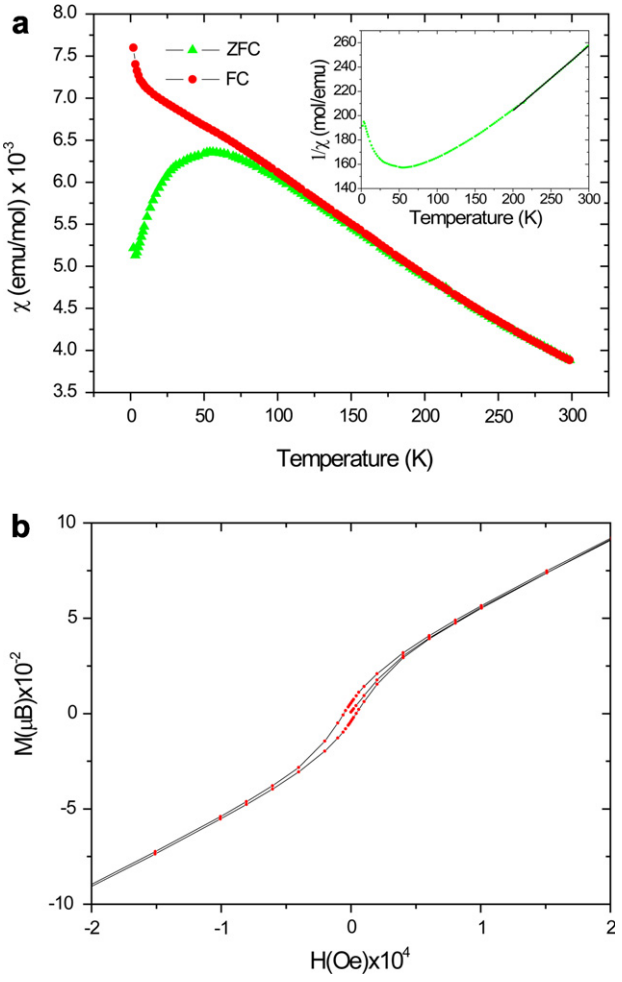

Fig. 7. a) Temperature dependence of the magnetic susceptibilities χ of $BiFeO_3$ at 1000 Oe. ZFC and FC curves are indicated by green triangles and red circles respectively. Inset: Inverse susceptibility $1/\chi$. The black solid line represents the fit of the data to the Curie–Weiss law. b) Magnetization vs applied magnetic field hysteresis loop of $BiFeO_3$ at 5 K. (For interpretation of the references to colour in this figure legend, the reader is referred to the web version of this article.)

The fitting procedure yielded: $C = 1.9$ and $\theta = -181$ K corresponding to a magnetic moment of 3.9 μ_B. Fig. 7b plots magnetization data collected at 5 K confirming that these samples show spontaneous magnetization not reaching saturation, which indicates a weak ferromagnetic nature [33,34]. Weak ferromagnetism has been suggested by early magnetic measurements but has not been definitely established [35,36].

4. Conclusion

In this communication we describe the structural, microstructural and Mössbauer characterization of a pure sample of $BiFeO_3$ prepared by a novel low-temperature method: microwave-hydrothermal synthesis. The X-ray data can be refined in two symmetries (R3c or Cc) with similar reliability factors. TEM and associated techniques have been employed as fundamental tools to investigate this material. The composition and homogeneity of the sample is determined by XEDS and to elucidate the true space group micro-diffraction analyses, which are performed in single crystals from a polycrystalline material and is sensitive to the symmetry, have been employed following the methodology described by Mornirolli et al. Once the R3c space group has been determined, the microstructure of our material has been studied by HRTEM showing a well-ordered material free of extended defects. This order is also detected in the oxygen sub-lattice imaged in the phase of the reconstructed exit wave. The presence of two hyperfine magnetic fields revealed in the Mössbauer spectra are associated with average values of two perpendicular spin directions along a spin modulated spiral structure. The pristine sample shows evidence of a small fraction (~2%) of Fe^{2+} in low spin configuration that could provoke structural distortions that are reduced after oxygenation.

Acknowledgements

Authors acknowledge the financial support extended in Mexico by DGAPA, UNAM (PAPIIT No IN116610) and the travel facilities from the "Convenio UNAM-UCM" from Intercambio Académico, Coordinación de la Investigación Científica (UNAM). On the spanish side, the authors are indebted to Comunidad Autónoma de Madrid (S2009/PPQ-1626) and Spanish Micinn (MAT-2010-19460).

References

[1] W. Eerenstein, N.D. Mathur, J.F. Scott, Nature 442 (2006) 759–765.
[2] C. Michel, J.-M. Moreau, G.D. Achenbach, R. Gerson, W.J. James, Solid. State. Commun. 7 (1969) 701–704.
[3] T. Zhao, A. Scholl, F. Zavaliche, K. Lee, M. Barry, A. Doran, M.P. Cruz, Y.H. Chu, C. Ederer, N.A. Spaldin, R.R. Das, D.M. Kim, S.H. Baek, C.B. Eom, R. Ramesh, Nat. Mater 5 (2006) 823–829.
[4] M.S. Bernardo, T. Jardiel, M. Peiteado, A.C. Caballero, M. Villegas, J. Eur. Ceram. Soc. (2011). doi:10.1016/j.jeurceramsoc.2011.03.018.
[5] S. Saha, S.B. Krupanidhi, J. Appl. Phys. 87 (2000) 849–854.
[6] J. Jiang, J. Zou, M.N. Anjum, J. Yan, L. Huang, Y. Zhang, J. Chen, Solid State Sciences (2011). doi:10.1016/j.solidstatesciences.2011.07.008.
[7] S. Mandal, C.K. Ghosh, D. Sarkar, U.N. Maiti, K.K. Chattopadhyay, Solid State Sciences 12 (2010) 1803–1808.
[8] A. Srivastava, A. Gargand, F.D. Morrison, J. Appl. Phys. 105 (2009) 054103–054109.
[9] R. Mazumder, D. Chakravarty, D. Bhattacharya, A. Sen, Mat. Res. Bull 44 (2009) 555–559.
[10] P. Fischer, M. Polomska, I. Sosnowska, M. Szymanski, J. Phys. C: Solid. State. Phys. 13 (1980) 1931–1940.
[11] T.T. Carvalho, P.B. Tavares, Mater. Lett. 62 (24) (2008) 3984–3986.
[12] J. Yu, N. Koshikawa, Y. Arai, S. Yoda, H. Saitou, J. Cryst. Growth. 231 (2001) 568–576.
[13] H. Koizumi, N. Niizeki, T. Ikeda, J. Appl. Phys. 3 (1964) 495–496.
[14] I. Sosnowska, W. Schaefer, W. Kockelmann, K.H. Andersen, I.O. Troyanchuk, Appl. Phys. A 74 (2002) S1040–S1042 ICSD #97591.
[15] D.C. Arnold, K.S. Knight, F.D. Morrison, P. Lightfoot, Phys. Rev. Lett. 102 (2009) 027602–027606.

[16] J. Prado-Gonjal, M.E. Villafuerte-Castrejón, L. Fuentes, E. Morán, Mater. Res. Bull. 44 (2009) 1734–1737.
[17] S.K. Pradhan, J. Das, P.P. Rout, S.K. Das, D.K. Mishra, D.R. Sahu, A.K. Pradhan, V.V. Srinivasu, B.B. Nayak, S. Verma, B.K. Roul, J. Magn. Magn. Mater. 322 (2010) 3614–3622.
[18] A. Reyes, C. de la Vega, M.E. Fuentes, L. Fuentes, J. Eur. Ceram. Soc. 27 (2007) 3709–3711 ICSD #157424.
[19] R.J. Zeches, et al., Science 326 (2009) 977–980.
[20] R.A.M. Gotardo, I.A. Santos, L.F. Cótica, E.R. Botero, D. Garcia, J.A. Eiras, Scripta Materialia 61 (2009) 508–511.
[21] J. Rodriguez-Carvajal, J. Physica B 192 (1993) 55–69.
[22] http://www.ill.eu/sites/fullprof/.
[23] http://www.ccp14.ac.uk/ccp/web-mirrors/powdcell/a_v/v_1/powder/e_cell.html.
[24] IWFR Software (Version 1.0, February 2005, HREM Research Inc.).
[25] MacTempas Software (Version 2.3.7, Roar Kilaas).
[26] Recoil 1.05, K. Lagarec and D.G. Rancourt, 1998.
[27] T. Hahn, International Tables of Crystallography, fifth ed., vol. A, Kluwer Academic Publishers, Boston, 2002.
[28] Morniroli and Steeds, Ultramicroscopy 45 (1992) 219–239.
[29] A.V. Zalessky, A.A. Frolov, T.A. Khimich, A.A. Bush, V.S. Pokatilov, A.K. Zvezdin, Europhys. Lett. 50 (2000) 547–551.
[30] A. Palewicz, T. Szumiata, R. Przeniosło, I. Sosnowska, I. Margiolaki, Solid. State. Commun. 140 (2006) 359–363.
[31] J. T-Park, G.C. Papaefthymiou, A.J. Viescas, A.R. Moodenbaugh, S.S. Wong, Nano Letters 7 (3) (2007) 766–772.
[32] S. Basu, M. Pal, D. Chakravorty, J. Magn. Magn. Mater. 320 (2008) 3361.
[33] V. Fruth, L. Mitoseriu, D. Berger, A. Ianculescu, C. Matei, S. Preda, M. Zaharescu, Prog. Solid. State. Ch. 35 (2007) 193–202.
[34] F. Azough, R. Freer, M. Thrall, R. Cernik, F. Tuna, D. Collison, J. Eur. Ceram. Soc. 30 (2010) 727.
[35] J.M. Moreau, C. Michel, R. Gerson, W.J. James, J. Phys. Chem. Solids. 32 (1971) 1315.
[36] G.A. Smolenskii, V.M. Yudin, Soviet Physics e Solid State 6 (1965) 2936.